Mechanical Systems and Signal Processing 122 (2019) 192–205

Contents lists available at ScienceDirect

Mechanical Systems and Signal Processing

journal homepage: www.elsevier.com/locate/ymssp

A robust Bayesian methodology for damage localization in plate-like structures using ultrasonic guided-waves

Sergio Cantero-Chinchilla [a,d,*], Juan Chiachío [b], Manuel Chiachío [c], Dimitrios Chronopoulos [a], Arthur Jones [a]

[a] Institute for Aerospace Technology & The Composites Group, The University of Nottingham, NG7 2RD, United Kingdom
[b] Department of Naval Architecture, Ocean & Marine Engineering, University of Strathclyde, Glasgow G4 0LZ, United Kingdom
[c] Dept. Structural Mechanics & Hydraulics Engineering, University of Granada, 18001, Spain
[d] Aernnova Engineering Division S.A., Madrid 28034, Spain

ARTICLE INFO

Article history:
Received 31 July 2018
Received in revised form 5 November 2018
Accepted 10 December 2018

Keywords:
Bayesian inverse problem
Ultrasonic guided-waves
Time of flight
Damage localization
Multiple damage areas
Structural health monitoring

ABSTRACT

SHM methods for damage detection and localization in plate-like structures have typically relied on signal post-processing techniques applied to ultrasonic guided-waves. The time of flight is one of these signals features which has been extensively used by the SHM community for damage localization. One approach for obtaining the time of flight is by applying a particular time-frequency transform to capture the frequency and energy content of the wave at each instant of time. To this end, the selection of a suitable methodology for time-frequency transform among the many candidates available in the literature has typically relied on experience, or simply based on considerations about computational efficiency. In this paper, a full probabilistic method based on the Bayesian inverse problem is proposed to rigorously provide a robust estimate of the time of flight for each sensor independently. Then, the robust prediction is introduced as an input to the Bayesian inverse problem of damage localization. The results reveal that the proposed methodology is able to efficiently reconstruct the damage localization within a metallic plate without the need to assume a specific a priori time-frequency transform model.

1. Introduction

Damage reconstruction and localization in plate-like structures using guided-waves based SHM have been mainly addressed using post-processing techniques applied to ultrasonic signals [1]. The exploration of large areas with a small attenuation [2] is one of the most remarkable characteristics that has led industries, such as the aerospace industry, to focus on guided-waves (e.g. the "PAMELA" system [3–5]). Other approaches that use acoustic-based SHM methods to localize damage in thin-walled structures are also available nowadays. These can be broadly classified into (1) passive sensing diagnostics (PSD) and (2) active sensing diagnostics (ASD) techniques. In contrast to PSD techniques, which are based on sensors in "listening-mode" (e.g., acoustic emission) [6–12], ASD techniques for plate-like structures emit ultrasonic waves that interact with the structure and are measured by sensors [13]. Sparse or phased-array sensors' layouts are placed so that the structure is actively interrogated on demand, which confers higher accuracy and reliability [14]. Potential safety and economical implications in condition-based maintenance are extra-motivations for the use of this SHM technique.

* Corresponding author at: Institute for Aerospace Technology & The Composites Group, The University of Nottingham, NG7 2RD, United Kingdom.
E-mail address: Sergio.CanteroChinchilla1@nottingham.ac.uk (S. Cantero-Chinchilla).

https://doi.org/10.1016/j.ymssp.2018.12.021
0888-3270/

Nomenclature

a, b	scaling and time-shift factors
c	normalizing constant in Bayes' theorem
$D^{(k)}$	mean of the hyper-robust model for the k-th sensor
$\hat{\mathbf{d}}^{(k)}$	set of $\hat{d}_j$ in the k-th sensor
$\hat{d}_j^{(k)}$	first energy peak provided by the j-th TF model in the k-th sensor
$\tilde{d}^{(k)}$	first energy peak in the k-th sensor
$\mathbf{D}$	set of $D^{(k)}$ values for all the sensors
$\mathcal{D}^{(k)}$	signal acquired in the k-th sensor
e	model error of ellipse-based ToF model
$g_j(\cdot)$	j-th TF model
$h(t)$	window function
$\mathbf{m}$	model parameters of ellipse-based ToF model
$\mathcal{M}_j^{(k)}$	j-th TF model class for the k-th sensor
$\mathbf{M}$	set of model classes $\mathcal{M}_j^{(k)}$
N	number of sensors
N_m	number of model classes
N_i^A	number of samples in i-th annealing level
$\mathcal{N}(\cdot,\cdot)$	Gaussian distribution
$P(\cdot)$	probability
$p(\cdot)$	probability density
$q(\cdot)$	proposal PDF in MCMC sampling algorithms
r	acceptance rate for the MH algorithm
T_s	number of samples generated in MH algorithm
$\text{ToF}_{\mathcal{D}}^{(a-s)}$	measured ToF between actuator a and sensor s
$\text{ToF}_{M}^{(a-s)}$	modeled ToF between actuator a and sensor s
$\mathcal{U}(\cdot,\cdot)$	uniform distribution
v	mean of prior PDF of the velocity
V_{a-d}, V_{d-s}	wave propagation velocity in paths $a-d$ and $d-s$, respectively
$w_j^{(k)}$	weight of the j-th TF model class in the k-th sensor used in the hyper-robust model
$X(t)$	time series of the signal
X_a, Y_a	actuator coordinates
X_d, Y_d	damage position coordinates
X_s, Y_s	sensor coordinates
$\text{ToF}_{M}^{(a-s)}$	magnitude of the analytical signal
γ	threshold parameter for AIMS algorithm
ε	error term in TF model
ζ	number of state of the chain in M-H
$\mathbf{\Theta}$	set of possible values of the parameters in the BIP
$\boldsymbol{\theta}$	set of ToF model parameters including σ_e
ρ	scaling factor in the prior PDF of σ_ϵ
σ_ε	standard deviation of ε
σ_e	standard deviation of model error of ellipse-based ToF model
σ_M	MAP value of σ_ε
σ_v	standard deviation of prior PDF of the velocity
$\Psi(t)$	analyzing wavelet
$\omega_j(t)$	instantaneous frequency

Moreover, the need for autonomous techniques that provide accurate health state indicators is specially crucial for aerospace structures, which are based on a considerable number of critical structural components requiring frequent inspection. Once a damaged area is detected, i.e. through analysis of damage tolerance exceedance, proper operational decisions can be taken. Two general approaches are typically adopted for damage detection: (1) model-based inverse problems, whereby detailed damage information (e.g. the severity of damage as residual strength) [15] can be obtained from the measured signal at a considerable computational cost; and (2) inverse problems based on post-processed signal features, whereby other relevant information, e.g. the damage position or the damage severity, can be obtained more efficiently. With regards to the second approach, several damage reconstruction techniques have been reported in the literature [2,16–18]. Among them, the time-of-flight (ToF) has been extensively used as a signal feature for its efficiency in obtaining information about material properties along with damage localization using post-processing scattered signals.

Time-frequency (TF) representation techniques have been intensively used for the extraction of ToF as a signal feature. By TF representation, a frequency domain spectrum can be obtained at each instant of time [19], however the results slightly differ from each other depending on the adoption of the various approaches available in the literature. Amongst them, the Hilbert-Huang transform (HHT), the continuous wavelet transform (CWT), the short-time Fourier transform (STFT) and the Wigner-Ville distribution (WVD) [19–22], are some of the most commonly used techniques in ultrasonic guided-waves based SHM applications [23–25]. Typically, the selection of one among the available options has been based on the modeler's experience or based on specific TF resolution characteristics. However, the selection of an unappropriated model may result in a biased damage identification [26,27] due to the disparate model assumptions and hypotheses adopted for each of them. In other words, the choice of a particular TF approach instead of another one is subject to *epistemic* uncertainty (i.e., lack of knowledge). Moreover, ultrasound-based damage localization conveys other sources of uncertainty which are mostly related with the measurement system and physical properties of the material. They might produce unreliable damage predictions should these uncertainties are not properly considered and quantified within the calculations.

To partially address this modeling issue, a number of researchers have proposed the use of probability-based methods [28–30]. Among them, the Bayesian inverse problem (BIP) applied to ultrasound based damage localization is getting increasing attention within the SHM community, although it is still in its early stage. In [24], the BIP was successfully proven in localizing damage areas in aluminum plates. More recently, a BIP methodology to account for the anisotropy in the *group velocity* was proposed in [23] for composite laminates. Notwithstanding, there is still an evident need for a rigorous treatment of the uncertainty in modeling the damage localization using ultrasonic guided-waves based methods, overall when multiple damage locations are expected.

This paper proposes a multi-level Bayesian framework to rigorously account for the overall uncertainty in application to the problem of ultrasound-based damage localization using Lamb waves. The main novelty of this paper is that it provides a unified methodology to rationally address the problem of damage identification using ultrasounds from probabilistic Bayesian principles: first, the problem of TF model selection is addressed for a given experimental configuration based on *posterior probabilities* that assess the relative degree of belief [31] of a particular model over a set of candidates; then, the problem of damage identification and localization is carried out using a BIP based on signal features adopting a *hyper-robust* TF model resulted from the first assessment level. To this end, once the raw data have been acquired, two BIPs are hierarchically formulated for each piezoelectric (PZT) sensor so that the outcome of the model selection problem is used as input for damage localization, as shown in Fig. 1. In this framework, uncertainties coming from (1) material's mechanical properties, (2) measurement errors, and (3) epistemic uncertainty in the TF model due to the Heisenberg principle [19,30], are taken into account. The proposed approach relies on rigorous *probability-logic* assumptions for model class selection [32] and as such, it avoids experience-based decisions about the optimal post-processing technique. Here, probability is interpreted as a multi-valued logic that expresses the degree of belief of a proposition conditioned on the given information [33,32]. The methodology is applied in two case studies using aluminum plates with one and two damaged areas, respectively. For the particular problem of damage localization, the asymptotic independent Markov sampling (AIMS) [34,35] algorithm is adopted to solve the resulting Bayesian inverse problem, showing high efficiency in dealing with damage multi-modality. In general, the results show the efficiency of the proposed methodology in reconstructing the damage position in plate-like structures using guided-waves, while rigorously accounting for the modeling uncertainties in the reconstruction.

The remainder of the paper is organized as follows: Section 2 shows the TF models used in the proposed model selection problem. Section 3 comprises the probabilistic methodology used to obtain the robust estimate of the ToF for each sensor.

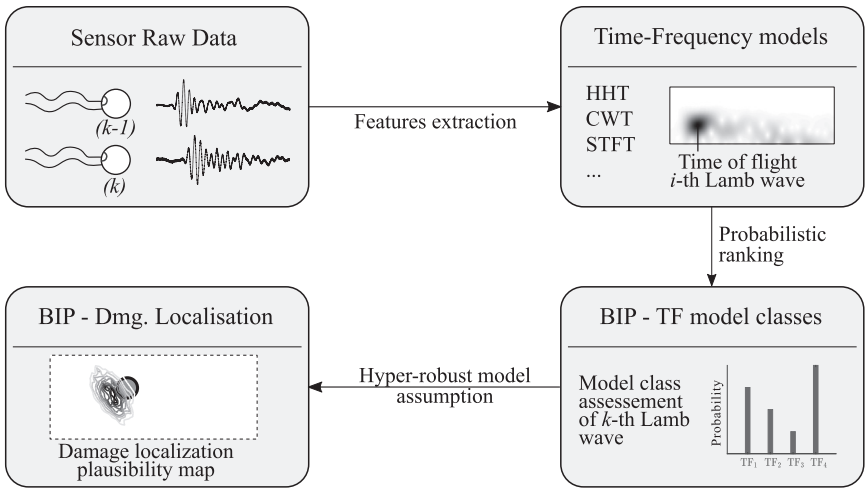

Fig. 1. General workflow proposed to address the challenge of damage localization. Note that the signal data can be obtained by numerical (e.g. FEM) or experimental methods (e.g. using PZT transducers, a signal generator, and an oscilloscope) [13].

The BIP principles used to obtain the damage localization are presented in Section 4. In Section 5, the proposed framework is applied in two case studies to serve as example. Section 6 discusses the robustness of the proposed methodology. Finally, Section 7 provides concluding remarks.

2. Time-frequency models

Among the most used TF models in the literature, four of them are selected in this paper to be assessed and ranked using the proposed Bayesian methodology for each sensor, independently; namely the HHT, CWT, STFT, and WVD. The main formulation of these TF representation techniques is shown in the following subsections.

2.1. Hilbert-Huang transform

The HHT is obtained by the sum of intrinsic mode functions (IMF) whereby the spectrum is defined after performing the Hilber transform over each IMF component [20,26], as follows:

$$g_1(t) = \sum_{j=1}^{n} \alpha_j(t) \exp\left(\mathrm{i} \int \omega_j(t)\ \mathrm{d}t\right) \tag{1}$$

where $\alpha_j(t)$ is the magnitude of the analytic signal which is typically considered as the envelope of the input time series or directly the signal acquired by the sensor, n is the number of IMF components, and $\omega_j(t)$ is the instantaneous frequency. Eq. (1) represents the amplitude and instantaneous frequency as function of time.

2.2. Continuous wavelet transform

TF wavelets are used in the CWT to obtain the TF representation of the assessed signal, by:

$$g_2(b,a) = \frac{1}{\sqrt{a}} \int_{-\infty}^{\infty} X(t) \overline{\Psi\left(\frac{t-b}{a}\right)} \mathrm{d}t \tag{2}$$

where $X(t)$ represents the time series of the signal, $\Psi(t)$ denotes the analysing wavelet, $a > 0$ is the scale factor, b is the time-shift variable, and the overline denotes the complex conjugate [21,36]. Remarkable time and frequency resolution are obtained using this model.

2.3. Short-time Fourier transform

Alternatively, the TF representation can be obtained with a STFT, which performs Fourier transforms to a moving window in the assessed signal [19,37], as follows:

$$g_3(\omega,t) = \frac{1}{2\pi} \int_{-\infty}^{\infty} e^{-\mathrm{i}\omega\tau} X(\tau) h(\tau - t) \mathrm{d}\tau \tag{3}$$

where $X(t)$ is the time series, $h(t)$ is a window function, and ω denotes the frequency. The energy spectrum of an STFT is known as a spectrogram.

2.4. Wigner-Ville distribution

The WVD can be interpreted as a measure of the signal's local time-frequency energy [37], and it is defined as follows:

$$g_4(\omega,t) = \int_{-\infty}^{\infty} X\left(t + \frac{\tau}{2}\right) \overline{X\left(t - \frac{\tau}{2}\right)} e^{-\mathrm{i}\omega\tau} \mathrm{d}\tau \tag{4}$$

where $X(t)$ is the time series and the overline denotes the complex conjugate. This technique is highly effective in detecting and localizing Dirac impulses and sinusoids [19,37].

3. Bayesian model class ranking

The TF models in Section 2 are just different alternatives based on a number of simplifying hypotheses and modeling assumptions to represent the same reality. Instead, for a particular model, the validity of such simplifying assumptions depends on the adopted values of certain model parameters (e.g. the dispersion parameter). Thus, to simultaneously identify both the plausibility of each TF model and the values of the model parameters that better suit the information coming from the raw ultrasonic data, a Bayesian inverse problem (BIP) is proposed here. Given a plate-like structure monitored through a set of PZT sensors, the BIP is addressed separately for each PZT sensor due to the potential differences between sensors, such as different working environments or manufacturing defects.

3.1. Stochastic embedding of TF models

Let us consider a candidate TF model defined by the relationship $g_j : \mathbb{R}^n \rightarrow \mathbb{R}$ between a discrete signal $\mathcal{D}^{(k)} \in \mathbb{R}^n$ acting as input and the model output $g_j \in \mathbb{R}$, where k denotes the k-th sensor in the structure. Next, let $\hat{d}_j^{(k)} \in \mathbb{R}$ be the first energy peak observed in the scattered ultrasound signal, so that $\hat{d}_j^{(k)} = g_j(\mathcal{D}^{(k)})$. Under the assumption that g_j is only a candidate model over a set of alternatives [32] (e.g. like those described in Section 2), then the measured first peak, denoted here as $\tilde{d}^{(k)}$, would be more rigorously represented as an uncertain variable, as follows:

$$\tilde{d}^{(k)} = g_j(\mathcal{D}^{(k)}) + \varepsilon \tag{5}$$

where ε is an uncertain error term which accounts for the discrepancy between $\hat{d}_j^{(k)}$ and $\tilde{d}^{(k)}$, namely the modeled and measured values for the first energy peak, respectively. Following the Principle of Maximum Information Entropy (PMIE) [32,33], this error can be conservatively assumed to be modeled as a zero-mean Gaussian distribution with standard deviation σ_ε, i.e., $\varepsilon \sim \mathcal{N}(0, \sigma_\varepsilon)$. The PMIE enables a rational way to establish a probability model for the model error term such that it produces the largest uncertainty (largest Shannon entropy); the selection of any other probability model would lead to an unjustified reduction in such uncertainty [32]. Thus, following Eq. (5), a probabilistic description of the TF model can be obtained as:

$$p\left(\tilde{d}^{(k)} | \mathcal{M}_j^{(k)}, \sigma_\varepsilon\right) = \left(2\pi\sigma_\varepsilon^2\right)^{-\frac{1}{2}} \exp\left(-\frac{1}{2}\left(\frac{\tilde{d}^{(k)} - g_j^{-1}(\mathcal{D}^{(k)})}{\sigma_\varepsilon}\right)^2\right) \tag{6}$$

where $\mathcal{M}_j^{(k)}$ denotes the j-th candidate *model class* within a set of N_m available TF models $\mathbf{M} = \left\{\mathcal{M}_1^{(k)}, \ldots, \mathcal{M}_j^{(k)}, \ldots, \mathcal{M}_{N_m}^{(k)}\right\}$. Each model class is defined by the stochastic TF model given by Eq. (6) along with the *prior* probability density function (PDF) of the model parameter σ_ε, $p\left(\sigma_\varepsilon | \mathcal{M}_j^{(k)}\right)$. This prior PDF represents the initial degree of belief of the values of σ_ε within a set of possible values $\boldsymbol{\Theta} \subseteq \mathbb{R}$ before the information from measurements is incorporated through Bayesian updating, as explained further below. For all the sensors in the structure, the stochastic model is defined independently, thus accounting for different potential sources of errors and uncertainties.

3.2. Model parameters estimation

Previously to obtain the model parameter updating from measurements, a preliminary assessment of the influence of the dispersion parameter σ_ε in the model class assessment and ranking was carried out, which showed a relatively high sensitivity of the resulting model class assessment to the value of this parameter. Thus, a first stage of the BIP is conceived to obtain the set of most plausible values for σ_ε given a set of data $\hat{\mathbf{d}}^{(k)} = \left\{\hat{d}_1^{(k)}, \ldots, \hat{d}_{N_m}^{(k)}\right\}$, which corresponds to a set of N_m values obtained by adopting each TF model class. To this end, the posterior PDF $p\left(\sigma_\varepsilon | \hat{\mathbf{d}}^{(k)}, \mathcal{M}_j^{(k)}\right)$ of the dispersion parameter σ_ε given the j-th TF model class ($\mathcal{M}_j^{(k)}$), is required. Thus, by using Bayes' theorem, this posterior PDF is given by:

$$p\left(\sigma_\varepsilon | \hat{\mathbf{d}}^{(k)}, \mathcal{M}_j^{(k)}\right) = c^{-1} p\left(\hat{\mathbf{d}}^{(k)} | \sigma_\varepsilon, \mathcal{M}_j^{(k)}\right) p\left(\sigma_\varepsilon | \mathcal{M}_j^{(k)}\right) \tag{7}$$

where c is a normalizing constant, so that:

$$\int_{\boldsymbol{\Theta}} p\left(\sigma_\varepsilon | \hat{\mathbf{d}}^{(k)}, \mathcal{M}_j^{(k)}\right) d\sigma_\varepsilon = \int_{\boldsymbol{\Theta}} c^{-1} p\left(\hat{\mathbf{d}}^{(k)} | \sigma_\varepsilon, \mathcal{M}_j^{(k)}\right) p\left(\sigma_\varepsilon | \mathcal{M}_j^{(k)}\right) d\sigma_\varepsilon = 1 \tag{8}$$

In Eq. (7), $p\left(\hat{\mathbf{d}}^{(k)} | \sigma_\varepsilon, \mathcal{M}_j^{(k)}\right)$ is the likelihood function, which expresses how likely the data $\hat{\mathbf{d}}^{(k)}$ are reproduced by the stochastic model in Eq. (6) if model class $\mathcal{M}_j^{(k)}$ is adopted, as shown in Fig. 2. This likelihood function can be obtained by substitution of the values of $\hat{\mathbf{d}}^{(k)}$ as the output of the stochastic model, as follows:

$$p\left(\hat{\mathbf{d}}^{(k)} | \sigma_\varepsilon, \mathcal{M}_j^{(k)}\right) = \prod_{\ell=1}^{N_m} p\left(\hat{d}_\ell^{\,(k)} | \sigma_\varepsilon, \mathcal{M}_j^{(k)}\right) \tag{9}$$

Therefore, Eq. (7) rewrites as:

$$p\left(\sigma_\varepsilon | \hat{\mathbf{d}}^{(k)}, \mathcal{M}_j^{(k)}\right) \propto \left\{\prod_{\ell=1}^{N_m} p\left(\hat{d}_\ell^{\,(k)} | \sigma_\varepsilon, \mathcal{M}_j^{(k)}\right)\right\} p\left(\sigma_\varepsilon | \mathcal{M}_j^{(k)}\right) \tag{10}$$

Furthermore, it is observed that the evaluation of the normalizing constant c in Eq. (7) cannot usually be evaluated analytically except for special cases based upon linear models and Gaussian uncertainties [38]. However, stochastic simulation

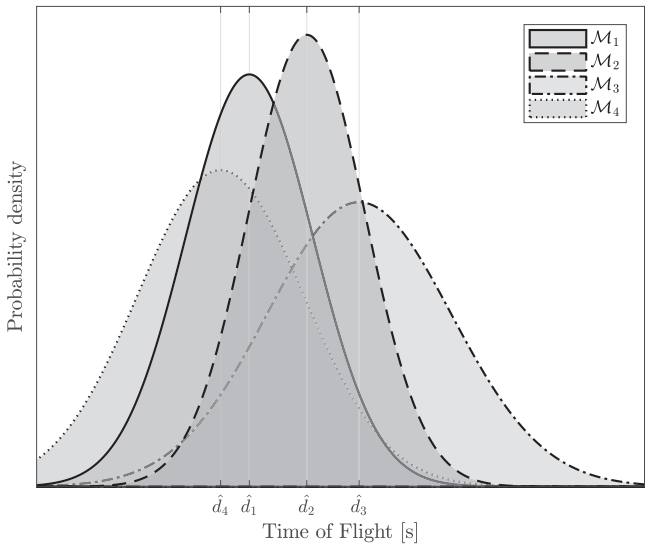

Fig. 2. Likelihood functions derived from each time-of-flight ($\hat{d}_j^{(k)}$). The standard deviation provided by *level I* of the proposed model ranking is expected to have different values in each model-class. The time-of-flight data are then substituted in the likelihood function $p\left(\hat{\mathbf{d}}^{(k)}|\sigma_\varepsilon, \mathcal{M}_j^{(k)}\right)$.

based on MCMC methods [39,40] can be used to obtain samples from the posterior avoiding the evaluation of c, as shown in the next section.

3.3. Model class assessment

The probabilistic approach for model class assessment is motivated by the uncertainty about the TF model based on the assumed hypotheses and simplifications adopted for its formulation [32,33]. Once the posterior $p\left(\sigma_\varepsilon|\hat{\mathbf{d}}^{(k)}, \mathcal{M}_j^{(k)}\right)$ is obtained, the plausibility of the model class $\mathcal{M}_j^{(k)}$ can be obtained by applying the Total Probability Theorem as:

$$\begin{aligned} P\left(\mathcal{M}_j^{(k)}|\hat{\mathbf{d}}^{(k)}\right) &= \int_{\boldsymbol{\Theta}} P\left(\mathcal{M}_j^{(k)}|\hat{\mathbf{d}}^{(k)}, \sigma_\varepsilon\right) p\left(\sigma_\varepsilon|\hat{\mathbf{d}}^{(k)}\right) d\sigma_\varepsilon \\ &= \int_{\boldsymbol{\Theta}} \frac{p\left(\hat{\mathbf{d}}^{(k)}|\mathcal{M}_j^{(k)}, \sigma_\varepsilon\right) P\left(\mathcal{M}_j^{(k)}|\mathbf{M}\right)}{\sum_{\ell=1}^{N_m} p\left(\hat{\mathbf{d}}^{(k)}|\mathcal{M}_\ell^{(k)}, \sigma_\varepsilon\right) P\left(\mathcal{M}_\ell^{(k)}|\mathbf{M}\right)} p\left(\sigma_\varepsilon|\hat{\mathbf{d}}^{(k)}\right) d\sigma_\varepsilon \end{aligned} \tag{11}$$

where $p\left(\sigma_\varepsilon|\hat{\mathbf{d}}^{(k)}\right)$ denotes the posterior PDF obtained by Eq. (10). Eq. (11) can be simplified by applying the asymptotic Laplace's approximation [32] as follows:

$$P\left(\mathcal{M}_j^{(k)}|\hat{\mathbf{d}}^{(k)}\right) \approx \frac{p\left(\hat{\mathbf{d}}^{(k)}|\mathcal{M}_j^{(k)}, \sigma_{M_j}\right) P\left(\mathcal{M}_j^{(k)}\right)}{\sum_{\ell=1}^{N_m} p\left(\hat{\mathbf{d}}^{(k)}|\mathcal{M}_\ell^{(k)}, \sigma_{M_j}\right) P\left(\mathcal{M}_\ell^{(k)}\right)} \tag{12}$$

where the conditioning on $\mathbf{M}$ has been suppressed for simplicity, and σ_{M_j} is the maximum a posteriori (MAP) value of the posterior PDF $p\left(\sigma_\varepsilon|\hat{\mathbf{d}}^{(k)}, \mathcal{M}_j^{(k)}\right)$, i.e.:

$$\sigma_M = \arg\max_{\sigma_\varepsilon} p\left(\sigma_\varepsilon|\hat{\mathbf{d}}^{(k)}, \mathcal{M}_j^{(k)}\right) \tag{13}$$

3.4. Hyper-robust model estimation

The probability-based ranking of the model classes $\mathcal{M}_j^{(k)}$ obtained above provides information about the degree of belief of the j-th TF model class for each sensor. However, a *hyper-robust* model [32] is proposed to account for the uncertainties held by all the model classes, thus providing a rigorous tool to address the model class selection. The hyper-robust model for a specific sensor k is defined as a weighted average of each TF model as follows:

$$p\left(\tilde{d}^{(k)}|\mathbf{M}\right) = \sum_{\ell=1}^{N_m} p\left(\tilde{d}^{(k)}|\mathcal{M}_\ell^{(k)}, \sigma_{M_\ell}\right) P\left(\mathcal{M}_\ell^{(k)}|\hat{\mathbf{d}}^{(k)}\right) \cong \mathcal{N}\left(\sum_{\ell=1}^{N_m} w_\ell^{(k)} \hat{d}_\ell^{(k)}, \sum_{\ell=1}^{N_m} \left(w_\ell^{(k)} \sigma_{M_\ell}\right)^2\right) \tag{14}$$

where $\tilde{d}^{(k)}$ are the possible ToF values and $w_\ell^{(k)}$ are the weights, given by the posterior probabilities of the ℓ-th model class $P\left(\mathcal{M}_\ell^{(k)}|\tilde{\mathbf{d}}^{(k)}\right)$. Given that each stochastic model is assumed to be distributed as a Gaussian function, a simplified expression for the hyper-robust Gaussian distribution is also provided in Eq. (14). However, to address the damage localization problem, the use of a stochastic model as the input data would require an intensively computational effort. Instead, the mean value of the hyper-robust model in the k-th sensor, denoted as $D^{(k)}$, is adopted.

4. Bayesian damage localization

4.1. Probabilistic description of ToF model

In this section, the damage localization is addressed by a model-based BIP using an ellipse-based ToF model [28], which has been extensively used for damage localization in guided-waves based SHM. For this problem, N_p actuator-sensor paths are considered in a plate-like structure to excite and receive Lamb waves for damage localization by screening changes of their ToF. To this end, the ToF information of the scattered signals can be theoretically obtained as follows [41]:

$$\mathrm{ToF}^{(a-s)} = \frac{\sqrt{(X_d - X_a)^2 + (Y_d - Y_a)^2}}{V_{a-d}} + \frac{\sqrt{(X_d - X_s)^2 + (Y_d - Y_s)^2}}{V_{d-s}} \tag{15}$$

where (X_d, Y_d) are the coordinates of the damage, (X_a, Y_a) are the actuator transducer coordinates, (X_s, Y_s) are the coordinates of one arbitrary sensor transducer, and V_{a-d} and V_{d-s} are the wave propagation velocities of the actuator-damage and damage-sensor paths respectively. These velocities are the same under the assumption of isotropic materials and a concentrated damage within a bounded region, i.e. $V = V_{a-d} = V_{d-s}$. Alternatively, under the consideration of orthotropic materials, such as composite structures, both velocity terms would be dependent on the angle of the actuator-damage and damage-sensor paths, $V_{a-d}(\alpha_a)$ and $V_{d-s}(\alpha_s)$ respectively [23].

To probabilistically describe the ToF model given by Eq. (15), uncertainties coming from the data, material properties, and also from the model itself, need to be accounted for. To this end, a set of uncertain model parameters $\mathbf{m} = \{X_d, Y_d, V\}$ are considered in this problem to describe the uncertainty about the damage coordinates as well as the wave propagation velocity. The set $\mathbf{m}$ of model parameters is augmented with a model error term $e \in \mathbb{R}$, resulting in a set of model parameters defined as $\boldsymbol{\theta} = \{\mathbf{m}, \sigma_e\} = \{X_d, Y_d, V, \sigma_e\} \in \boldsymbol{\Theta}$, where σ_e is the standard deviation of the error term e and $\boldsymbol{\Theta}$ is the model parameter space. This set of parameters is further updated through Bayes' Theorem, as will be explained below. The referred model error term $e \in \mathbb{R}$ is considered to account for the non-existence of a theoretical ToF model that fully represent the reality, so that:

$$\mathrm{ToF}_{\mathcal{D}}^{(a-s)} = \mathrm{ToF}_{M}^{(a-s)}(\mathbf{m}) + e = \mathrm{ToF}_{M}^{(a-s)}(\boldsymbol{\theta}) \tag{16}$$

where subscripts M and $\mathcal{D}$ from $\mathrm{ToF}_{M}^{(a-s)}$ and $\mathrm{ToF}_{\mathcal{D}}^{(a-s)}$ refer to modeled and measured ToF, respectively. Note in Eq. (16) that e provides the discrepancy between $\mathrm{ToF}_{M}^{(a-s)}$ and $\mathrm{ToF}_{\mathcal{D}}^{(a-s)}$ values. By the PMIE, this error term can be conservatively described as a zero-mean Gaussian distribution with covariance σ_e as $\mathcal{N}(0, \sigma_e)$. Thus, a probabilistic description of the ToF model from Eq. (16) can be obtained as:

$$p\left(\mathrm{ToF}_{\mathcal{D}}^{(a-s)}|\mathrm{ToF}_{M}^{(a-s)}(\boldsymbol{\theta})\right) = \left(2\pi\sigma_e^2\right)^{-\frac{1}{2}} \exp\left(-\frac{1}{2}\left(\frac{\mathrm{ToF}_{\mathcal{D}}^{(a-s)} - \mathrm{ToF}_{M}^{(a-s)}(\boldsymbol{\theta})}{\sigma_e}\right)^2\right) \tag{17}$$

Observe that Eq. (17) provides a measurement of the similarity of the modeled and measured ToF. Also, note that Eq. (17) provides a likelihood function for the $\mathrm{ToF}_{\mathcal{D}}^{(a-s)}$ data under the $\mathrm{ToF}_{M}^{(a-s)}(\boldsymbol{\theta})$ model.

4.2. Model parameter estimation

Given the likelihood function in Eq. (17), one can obtain the posterior PDF of the model parameters given the ToF data $\mathbf{D} = \left\{D^{(1)}, \ldots, D^{(N)}\right\}$, where N is the total number of sensors by applying the well-known Bayes' Theorem as:

$$p(\boldsymbol{\theta}|\mathbf{D}) = \frac{p(\mathbf{D}|\boldsymbol{\theta})p(\boldsymbol{\theta})}{p(\mathbf{D})} \tag{18}$$

where $p(\boldsymbol{\theta})$ is the prior PDF of the model parameters, and $p(\mathbf{D}|\boldsymbol{\theta})$ is the likelihood function for the set of data $\mathbf{D}$. Given the stochastic independence of the measurements, the likelihood can be expressed as $p(\mathbf{D}|\boldsymbol{\theta}) = \prod_{k=1}^{N} p\left(D^{(k)}|\boldsymbol{\theta}\right)$, where each factor $p\left(D^{(k)}|\boldsymbol{\theta}\right)$ is given by Eq. (17). Finally, $p(\mathbf{D})$ is the evidence of the data under the model specified by $\boldsymbol{\theta}$. This term, which acts as a normalizing factor within the Bayes' theorem, can be bypassed through sampling, e.g. using Markov Chain Monte Carlo (MCMC) methods [42]. Thus, Eq. (18) can be rewritten as:

$$p(\boldsymbol{\theta}|\mathbf{D}) \propto \left\{\prod_{k=1}^{N} p\left(D^{(k)}|\boldsymbol{\theta}\right)\right\} p(\boldsymbol{\theta}) \tag{19}$$

4.3. Asymptotic independence Markov sampling algorithm

Algorithm 1 Pseudo-code implementation of AIMS algorithm.

1: `Preamble` Define $\gamma \in \mathbb{R}$ ▷{threshold for the essential sampling size (ESS)}, $N_0^A, \ldots, N_j^A, \ldots, N_m^A$ ▷{total number of samples in each annealing level j}, $q_0(\cdot|\theta), \ldots, q_j(\cdot|\theta), \ldots, q_m(\cdot|\theta)$ ▷{proposal distributions at each annealing level j}
2: `Algorithm`
3: $j = 0$ ▷{first annealing level}
4: Sample $\left\{\theta_0^{(i)}\right\}_{i=1}^{N_0^A}$, where $\theta_0^{(i)} \sim p(\boldsymbol{\theta})$
5: Obtain the ESS as a measure of the similarity between $p_0(\cdot)$ and the target distribution $p(\cdot)$
6: **while** ESS$/N_j < \gamma$ **do**
7: Obtain the normalized importance weights as a measure of the relative importance of the likelihood function in annealing levels $j+1$ and j [34].
8: Run the M-H algorithm to generate N states of a Markov chain with target distribution $p_{j+1}(\cdot)$: Generate a Markov chain $\theta_{j+1}^{(1)} \ldots \theta_{j+1}^{(N_{j+1}^A)}$ with target distribution $p_{j+1}(\cdot)$ [34].
9: Calculate the ESS as a measure of the similarity between $p_{j+1}(\cdot)$ and the target $p(\cdot)$
10: $j \leftarrow j+1$
11: **end while**
12: Set $m = j+1$ ▷{total number of steps in the annealing approach}
13: Generate a Markov chain $\theta_m^{(1)} \ldots \theta_m^{(N_m^A)}$ with distribution $p_m(\cdot) = p(\cdot)$ at annealing level m.

In practice, the presence of multiple damage locations in plate-like structures is possible, thus the updating algorithm used to obtain the posterior PDF of the locations of such potential damage should be able to provide samples of a multimodal PDF. In the literature, the majority of available MCMC algorithms can identify multimodal posterior PDFs at the cost of increasing the computational burden, which can be exacerbated if large dimensional parameter spaces are explored, or by introducing *ad hoc* algorithmic modifications [43]. To overcome this drawback, the asymptotic independence Markov sampling (AIMS) algorithm [34] is used here due to its efficiency to provide samples from multi-modal posterior PDFs. In AIMS algorithm, a posterior PDF $p(\cdot)$ is approximated using a combination of three well-known stochastic simulation methods. To this end, *simulated annealing* is used to obtain the target distribution $p(\cdot)$ from the prior distribution by sampling intermediate distributions $p_j(\cdot)$ through a *random walk M-H*. The intermediate distributions $p_j(\cdot)$ are approximated by using *importance sampling*. A pseudo-code implementation of AIMS method is provided as Algorithm 1.

5. Case studies

In this section, two case studies are presented to validate the proposed model class selection methodology using a set of guided-waves synthetically generated by finite element modeling (FEM). The methodology is applied to two cases of damage detection and localization considering one and two damaged areas, respectively.

5.1. Synthetic signal generation

To numerically generate the input signals, Lamb waves are modeled using Abaqus® for the simulations. The waves are generated over a thin plate made of aluminum-based alloy 2024-T351 with dimensions 0.5 m × 0.25 m, as depicted in Fig. 3 (see further properties about the aluminum alloy 2024-T351 in Table 1). In Fig. 3 (panel (a)), sensor numbering is established starting from S1 for the left-most upper sensor to S14 for the right-most down sensor. In panel (b), which corresponds to the case of two damage locations, sensors are analogously arranged starting from S1 to S6. For the ToF calculations, the Abaqus/Explicit module is used in this work for its effectiveness in simulating the transient behavior of the ultrasonic guided-waves.

A 4-node, quadrilateral, stress-displacement shell element with reduced integration and a large-strain formulation, referred to as S4R element [45], is used for the plate model, which is uniformly meshed using square elements of 1 mm size. The element size is determined by the smallest wavelength λ_{min} of the guided-wave mode represented. A minimum of 10 nodes per wavelength is normally required to ensure the avoidance of spatial aliasing [46]. The signal excitation is modeled as a perpendicular point force generated as a sine tone-burst of 5 cycles centered at a frequency $f = 100$ kHz. This frequency

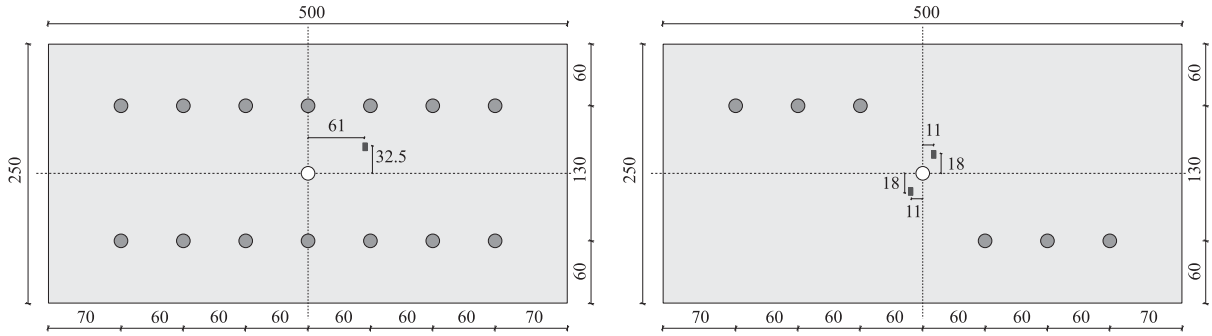

(a) Case study 1 considering one damage locations and 14 sensors. (b) Case study 2 considering two damage locations and 6 sensors.

Fig. 3. Representation of the aluminum plates considered in both case studies along with the position and layout of the sensors (dimensions expressed in millimetres). The white circle represents the actuator, which is positioned in the center of the plate. Damage is represented using dark rectangles.

Table 1
Material and structural properties (aluminum alloy 2024-T351 [44]) used in the Abaqus model.

Young's modulus [GPa]	Poisson's ratio [–]	Density [kg/m^3]	Thickness [mm]
73.1	0.33	2780	1.5

is selected to avoid extra complexity in the signal post-processing due to the appearance of possible higher order guided-waves modes. When the frequency is maintained at relatively low values, only both anti-symmetric 0 (A0) and symmetric 0 (S0) modes are excited [46]. Given that the wave propagation velocity of the mode[1] captured by the model is around $V = 1950$ m/s, the maximum element size would be $\lambda/10 = (V/f)/10 = 1.95$ mm. However, note that the selected element size (1 mm) is nearly half of the maximum value. Next, the damage is modeled as a rectangular hole of dimension 2 mm $\times$ 4 mm for both case studies considered in this paper. Free boundary conditions are considered in both cases. The ultrasonic signals are then received by the sensors in both undamaged and damaged cases. Afterwards, signals from both states are subtracted, thus the scattered information from the damage is obtained, as described in Section 4.1.

5.2. Model selection results

As previously mentioned, the simulated response of the plate to Lamb waves is used as data within the Bayesian framework. First, the standard deviation parameter σ_ε is defined as $\sigma_\varepsilon = \rho \cdot \hat{d}_j^{(k)}$, where $\hat{d}_j^{(k)}$ is the time of arrival at the k-th sensor using the j-th TF model, and ρ is a factor defined within a sufficiently large interval, which in this example is taken as $(0, 0.5]$. Therefore, the prior PDF of σ_ε can be expressed as a uniform distribution over the referred interval, i.e. $p(\sigma_\varepsilon) = \mathcal{U}\left(0, 0.5 \cdot \hat{d}_j^{(k)}\right)$. The posterior PDF $p\left(\sigma_\varepsilon | \hat{\mathbf{d}}^{(k)}, \mathcal{M}_j^{(k)}\right)$ is obtained through samples using the Metropolis-Hasting (M-H) algorithm (see a pseudo-code implementation in Appendix A) with $T_s = 40,000$ and a Gaussian *proposal distribution*, i.e., $q(\theta'|\theta) = \mathcal{N}(\theta, \sigma)$, where σ is the standard deviation of the M-H random walk which is selected such that the acceptance rate r lies within the interval $[0.2, 0.4]$ [47–49]. The maximum a posteriori (MAP) parameter is then computed and introduced as an input for the model class selection problem, as explained in Section 3.3.

The resulting posterior probabilities from Eq. (12) are subsequently used to rank the candidate TF models for each of the sensors, as shown in Figs. 4a and b for case study 1 and 2, respectively. Observe from these results that there is not a particularly predominating TF model for all the sensors. Nonetheless, the CWT model emerges as the most plausible one for a considerable majority of sensors, i.e., 8 out of 14 sensors for the case study 1, and 4 out of 6, for case study 2. Therefore, if a single TF model had to be selected for damage identification, a rational selection based on these results would be to choose the CWT model, since the better representation of the given data for the majority of sensors is provided by this choice. This output is in agreement with most of the authors in the literature who select CWT model to obtain the ToF from the scattered signals [23,24]. Notwithstanding, a hyper-robust model can be obtained by applying Eq. (14) using the posterior probabilities of each model class. The ToFs in this case are obtained by a model average from the probabilistic model from each sensor, as shown in Table 2. These values are subsequently used to reconstruct the damage in the BIP of damage localization, which is shown next.

[1] The referred mode is the anti-symmetric mode (A0) since only the bending mode can be captured with shell elements.

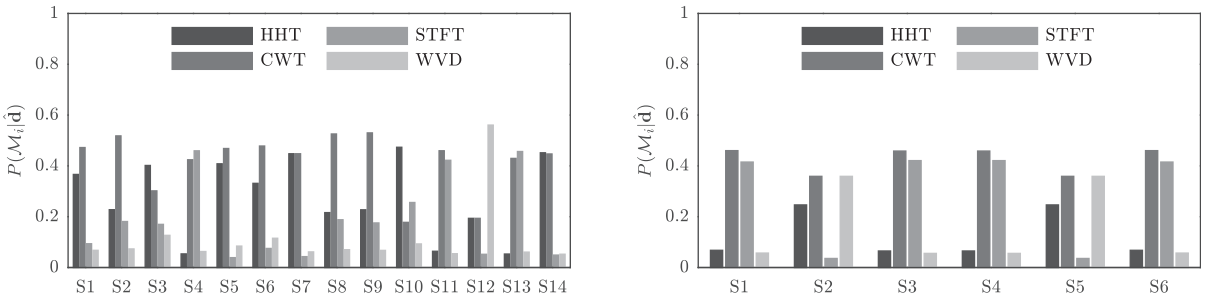

(a) $P(\mathcal{M}_i|\hat{\mathbf{d}})$ for case study 1 (b) $P(\mathcal{M}_i|\hat{\mathbf{d}})$ for case study 2

Fig. 4. Posterior probability $P\left(\mathcal{M}_i|\hat{\mathbf{d}}\right)$.

Table 2
Time of arrival ($D^{(k)}$) obtained as the mean of the hyper-robust models given by Eq. (14).

	Sensor	Time $D^{(k)}$ [μs]	Sensor	Time $D^{(k)}$ [μs]
Case study 1	S1	157.53	S8	163.33
	S2	125.29	S9	136.23
	S3	98.125	S10	114.66
	S4	71.539	S11	94.115
	S5	49.164	S12	83.664
	S6	70.242	S13	96.235
	S7	98.500	S14	116.35
Case study 2	S1	109.96	S4	54.577
	S2	81.214	S5	81.214
	S3	54.577	S6	109.96

5.3. Damage localization and reconstruction

Once the TF models are ranked and the hyper-robust TF model is obtained, the mean values of each hyper-robust model for each sensor are used as ToF data **D** within the BIP of damage localization, described in Section 4. The prior information of the model parameters has been defined as a uniform distribution for the damage position and dispersion parameter ($X \sim \mathcal{U}(-0.25, 0.25)$ m, $Y \sim \mathcal{U}(-0.125, 0.125)$ m, and $\sigma_e \sim \mathcal{U}(0, 10^{-4})$), and a Gaussian PDF for the velocity $V \sim \mathcal{N}(v, \sigma_v)$, where $v = 1950$ m/s and $\sigma_v = 40$ m/s. The posterior PDF of model parameters $\boldsymbol{\theta}$ is obtained in this case using the AIMS algorithm, with a threshold value $\gamma = 1/2, 10^5$ samples per annealing level, and a Gaussian PDF as proposal distribution, i.e. $q(\theta'|\theta) = \mathcal{N}(\theta, \sigma)$, where σ is the standard deviation of the M-H random walk which is again selected such that the acceptance rate r lies within the interval $[0.2, 0.4]$. Fig. 5 shows the inferred damage position for the aluminum plates of case study 1 and 2, respectively, using the hyper-robust TF model obtained by Eq. (14). The hyper-robust model is obtained for each sensor by

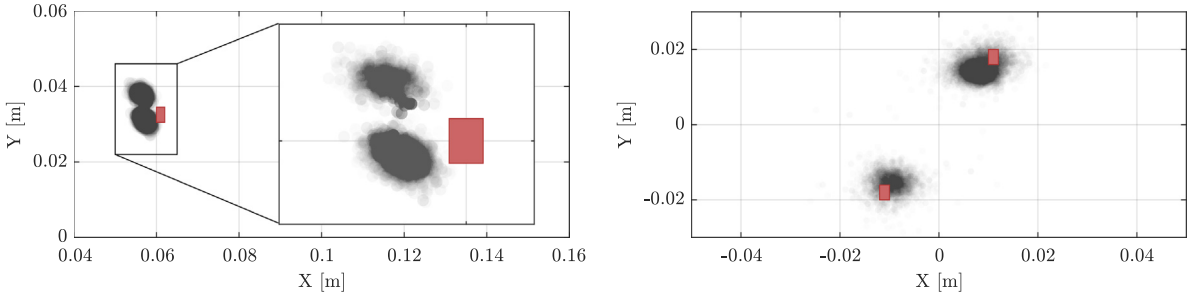

(a) Estimated and actual damage position ($X-Y$) for the case study 1 (b) Estimated and actual damage position ($X-Y$) for the case study 2

Fig. 5. Damage location estimation for the plate of case study 1 and 2. The actual position of the center of the damage is depicted using red rectangles which are represented in actual dimensions. (For interpretation of the references to colour in this figure legend, the reader is referred to the web version of this article.)

model averaging weighted using the posterior plausibilities of the TF models, showed in Fig. 4. It is observed that the damage position is efficiently reconstructed with the BIP methodology presented in this paper. The results also show that for the particular case study 2, the multi-modality due to dual damage position is well addressed using the AIMS algorithm.

The marginal posterior distributions of the other two parameters used by the BIP of damage localization, namely the standard deviation factor of the likelihood function σ_e and the wave propagation velocity V, are depicted in Fig. 6. In case study 1, a lower level of dispersion in both parameters, σ_e and V, is observed, whereas in case study 2, a higher dispersion is obtained.

6. Discussion

The proposed Bayesian methodology for damage localization has been exemplified using two case studies presented in Section 5. For each of the sensors, a Bayesian model class assessment framework is proposed to rank the candidate TF models, according to relative plausibilities that measure the relative degree of belief of the candidate model class in interpreting the raw signal acquired by the sensor. These relative plausibilities are then used to obtain a hyper-robust TF model for each sensor, which provides a higher level of robustness to damage localization than just taking the most plausible TF model among the candidate set. This robustness is clearly manifested in Fig. 5a, where damage position is identified in two plausible regions close to the actual damage position; an unjustified TF model choice would lead to a biased localization due to unconsidered model uncertainty. The same behavior can be also observed in Fig. 6b for the reconstruction of the wave propagation velocity parameter. Note that the ultrasonic data used in both case studies are synthetically obtained through FEM, although the methodology is entirely applicable to real ultrasonic signals. However, for real ultrasonic data, the uncertainty in the damage localization would be higher due to electronic noise or other measurement errors coming from, for instance, imperfect sensor bonding.

Then, a damage localization BIP using an ellipse-based model is applied to reconstruct the damage position using the AIMS algorithm as Bayesian updating algorithm. The data **D** are obtained by using the mean of the hyper-robust model, given by Eq. (14) for each sensor independently. The damage location has been remarkably inferred in both case studies. However, a higher dispersion in the $X-Y$ parameters (larger localization uncertainty) has been found in case study 2 compared to case study 1, as can be observed in Fig. 5. In addition, a higher dispersion is identified in the marginal distribution of the standard

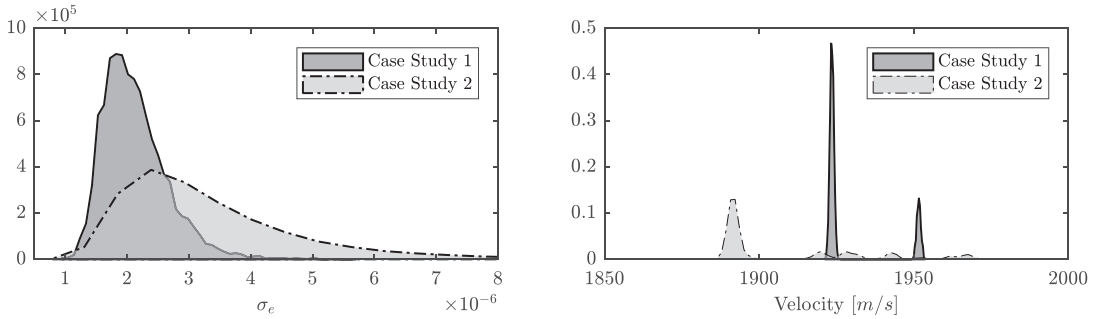

(a) Dispersion parameter (σ_e). (b) Wave propagation velocity (V).

Fig. 6. Posterior PDFs of the σ_e and V parameters for both case study 1 and 2.

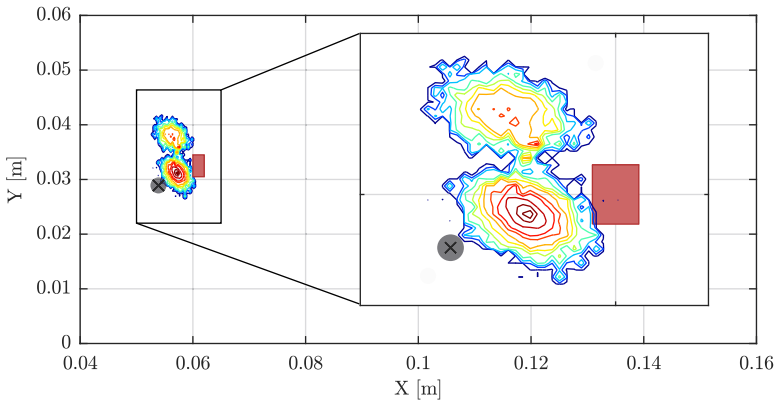

Fig. 7. Comparison between a deterministic damage localization using GA (grey point) and the results obtained with the proposed Bayesian methodology.

deviation parameter σ_e in case study 2. This could be explained due to the nature of the likelihood function from Eq. (17), which is a Gaussian distribution. In order to properly identify the two damage positions in this case study, the posterior values of σ_e (which is an updatable parameter) need to increase, hence leading to a higher dispersion in the damage localization as well as in the velocity parameter reconstruction, as observed in Fig. 6. This points out a limitation of the proposed methodology when dealing with multiple damage locations. In this context, a desirable further work would be the exploration of optimal likelihood functions to deal with damage multi-modality.

The robustness of the proposed methodology can then be observed by comparing the Bayesian identification results against those obtained using a deterministic approach. A well-known method to address inverse problems efficiently, but deterministically, is by the use of genetic algorithms (GA) [50]. GA's are used to find the value of the parameters that minimizes a *cost function*, which in this case can be defined as $\|\mathrm{ToF}_{\mathcal{D}}^{(a-s)} - \mathrm{ToF}_{M}^{(a-s)}(\mathbf{m})\|_2^2$, a L_2-norm of the residual time of flight between the model and the data. Fig. 7 depicts the comparison between the damage identification results obtained using the proposed Bayesian methodology and a deterministic GA-based inverse problem. To better highlight the robustness of the proposed Bayesian damage identification methodology in the presence of uncertainties, a bias is artificially introduced in the velocity term as a 5% of deviation in the value obtained through Abaqus (from 1950 m/s to 1850 m/s). Note that even with this small deviation, the damage localization results given by the GA become biased, whereas the results using Bayesian methodology are virtually immune to such variation. This simple example demonstrates the superiority of the proposed methodology in reconstructing the position of damage from guided-waves data, regardless of potential input errors.

Finally, it is worth mentioning that the position of the sensors plays a crucial role in the damage reconstruction. As observed in Fig. 3, case studies 1 and 2 have different sensor selection and layout. In this paper, a former sensitivity study on the sensors positions was carried out to identify: (1) the best number and (2) locations of sensors for each case study. Therefore, given the influence of the aforementioned two factors in the reconstruction of the damage position, an immediate further work will be the exploration of an efficient methodology for optimal sensor configuration, based on rigorous probabilistic assumptions to deal with the aforementioned sources of uncertainties.

7. Conclusions

A Bayesian methodology for damage location using guided-waves is presented in this paper. This methodology allows accounting for several sources of uncertainty, like the epistemic uncertainty due to TF model selection, and the uncertainty coming from the measurement noise and variable material properties. The effectiveness of the method is shown through two case studies with one and two damaged areas, respectively. The following conclusions are drawn from this paper:

- The damage position can be accurately reconstructed using ToFs proving the effectiveness of the proposed multi-level Bayesian inverse problem methodology;
- The use of a hyper-robust TF model as an input for the damage localization Bayesian inverse problem leads to a more robust damage inference;
- The reconstruction of the two damage areas in case study 2 (multi-modality) has been remarkably addressed by using the AIMS algorithm. However, under this scenario of damage, an important increase in the posterior uncertainty of the model parameters is obtained.

Further research work is under consideration with regards to: (1) the assessment of a suitable likelihood function to efficiently deal with multi-modal damage scenarios, (2) devising a rigorous technique for optimal sensor configuration in ultrasonic guided-waves based SHM, and (3) the influence of different types of damage in the performance of the proposed methodology.

Acknowledgements

This paper is part of the SAFE-FLY project that has received funding from the European Union's Horizon 2020 research and innovation programme under the Marie Skłodowska-Curie grant agreement No 721455.

Appendix A. Metropolis-Hastings simulation for Bayesian updating

The M-H algorithm generates samples from a specially constructed Markov chain whose stationary distribution is the required posterior PDF $p\left(\boldsymbol{\theta}|\hat{\mathbf{d}},\mathcal{M}\right)$. By sampling a candidate model parameter $\boldsymbol{\theta}'$ from a *proposal distribution* $q(\boldsymbol{\theta}'|\boldsymbol{\theta}^{\zeta})$, the M-H obtains the state of the chain at $\zeta+1$, given the state at ζ, specified by $\boldsymbol{\theta}^{\zeta}$. The candidate parameter $\boldsymbol{\theta}'$ is accepted (i.e., $\boldsymbol{\theta}^{\zeta+1}=\boldsymbol{\theta}'$) with probability $\min\{1,r\}$, and rejected (i.e., $\boldsymbol{\theta}^{\zeta+1}=\boldsymbol{\theta}^{\zeta}$) with the remaining probability $1-\min\{1,r\}$, where:

$$r=\frac{p\left(\hat{\mathbf{d}}|\boldsymbol{\theta}',\mathcal{M}\right)p(\boldsymbol{\theta}'|\mathcal{M})q\left(\boldsymbol{\theta}^{\zeta-1}|\boldsymbol{\theta}'\right)}{p\left(\hat{\mathbf{d}}|\boldsymbol{\theta}^{\zeta-1},\mathcal{M}\right)p(\boldsymbol{\theta}^{\zeta-1}|\mathcal{M})q\left(\boldsymbol{\theta}'|\boldsymbol{\theta}^{\zeta-1}\right)} \tag{A.1}$$

The process is repeated until T_s samples have been generated so that the monitored acceptance rate (ratio between accepted M-H samples over total amount of samples) reaches an asymptotic behaviour. A pseudo-code description of this method is provided below as Algorithm 2.

Algorithm 2 M-H algorithm.

1. Initialize $\boldsymbol{\theta}^{\zeta=0}$ by sampling from the prior PDF: $\boldsymbol{\theta}^0 \sim p(\boldsymbol{\theta}|\mathcal{M})$
for $\zeta = 1$ to T_s **do**
  2. Sample from the proposal: $\boldsymbol{\theta}' \sim q\left(\boldsymbol{\theta}'|\boldsymbol{\theta}^{\zeta-1}\right)$
  3. Compute r from Eq. (A.1)
  4. Generate a uniform random number: $\alpha \sim \mathcal{U}[0,1]$
  if $r \geqslant \alpha$ **then**
    5. Set $\boldsymbol{\theta}^{\zeta} = \boldsymbol{\theta}'$
  else
    6. Set $\boldsymbol{\theta}^{\zeta} = \boldsymbol{\theta}^{\zeta-1}$
  end if
end for

References

[1] J. Achenbach, Wave Propagation in Elastic Solids, North-Holland Publishing Company/American Elsevier, 1973.
[2] Z. Su, L. Ye, Y. Lu, Guided Lamb waves for identification of damage in composite structures: a review, J. Sound Vib. 295 (3–5) (2006) 753–780.
[3] G. Aranguren, P. Monje, V. Cokonaj, E. Barrera, M. Ruiz, Ultrasonic wave-based structural health monitoring embedded instrument, Rev. Sci. Instrum. 84 (12) (2013) 125106.
[4] P.M. Monje, L. Casado, G. Aranguren, V. Cokonaj, E. Barrera, M. Ruiz, Integrated electronic system for ultrasonic structural health monitoring, in: European workshop on structural health monitoring, 2012, pp. 1–8.
[5] A. Alcaide, E. Barrera, M. Ruiz, G. Aranguren, Damage detection on Aerospace structures using PAMELA SHM System, in: 6th International Symposium on NDT in Aerospace, Madrid, 2014.
[6] V. Giurgiutiu, Chapter 9 – impact and acoustic emission monitoring for aerospace composites SHM, in: V. Giurgiutiu (Ed.), Structural Health Monitoring of Aerospace Composites, Academic Press, Oxford, 2016, pp. 317–394.
[7] A. Tobias, Acoustic-emission source location in two dimensions by an array of three sensors, Non-destructive Testing 9 (1) (1976) 9–12.
[8] J. Park, F.-K. Chang, System identification method for monitoring impact events, Smart Structures and Materials 2005: Smart Sensor Technology and Measurement Systems, vol. 5758, International Society for Optics and Photonics, 2005, pp. 189–201.
[9] J.F. Markmiller, F.-K. Chang, Sensor network optimization for a passive sensing impact detection technique, Struct. Health Monit. 9 (1) (2010) 25–39.
[10] L.E. Mujica, J. Vehí, W. Staszewski, K. Worden, Impact damage detection in aircraft composites using knowledge-based reasoning, Struct. Health Monit. 7 (3) (2008) 215–230.
[11] C. Hiche, C.K. Coelho, A. Chattopadhyay, A strain amplitude-based algorithm for impact localization on composite laminates, J. Intell. Mater. Syst. Struct. 22 (17) (2011) 2061–2067.
[12] H. Fu, C.-M. Vong, P.-K. Wong, Z. Yang, Fast detection of impact location using kernel extreme learning machine, Neural Comput. Appl. 27 (1) (2016) 121–130.
[13] M. Mitra, S. Gopalakrishnan, Guided wave based structural health monitoring: a review, Smart Mater. Struct. 25 (5) (2016) 053001.
[14] L. Wang, F. Yuan, Active damage localization technique based on energy propagation of Lamb waves, Smart Struct. Syst. 3 (2) (2007) 201–217.
[15] J. Chiachío, N. Bochud, M. Chiachío, S. Cantero, G. Rus, A multilevel Bayesian method for ultrasound-based damage identification in composite laminates, Mech. Syst. Signal Process. 88 (2017) 462–477.
[16] C.H. Wang, J.T. Rose, F.-K. Chang, A synthetic time-reversal imaging method for structural health monitoring, Smart Mater. Struct. 13 (2) (2004) 415.
[17] J.E. Michaels, T.E. Michaels, Guided wave signal processing and image fusion for in situ damage localization in plates, Wave Motion 44 (6) (2007) 482–492.
[18] J.E. Michaels, A.J. Croxford, P.D. Wilcox, Imaging algorithms for locating damage via in situ ultrasonic sensors, in: Sensors Applications Symposium, 2008. SAS 2008. IEEE, IEEE, 2008, pp. 63–67.
[19] L. Cohen, Time-frequency Analysis: Theory and Applications, Prentice-Hall Inc, Upper Saddle River, NJ, USA, 1995.
[20] N.E. Huang, Z. Shen, S.R. Long, M.C. Wu, H.H. Shih, Q. Zheng, N.-C. Yen, C.C. Tung, H.H. Liu, The empirical mode decomposition and the Hilbert spectrum for nonlinear and non-stationary time series analysis, Proceedings of the Royal Society of London A: mathematical, physical and engineering sciences, vol. 454, The Royal Society, 1998, pp. 903–995.
[21] C.K. Chui, An Introduction to Wavelets, Academic Press Professional Inc, San Diego, CA, USA, 1992.
[22] C. Bao, H. Hao, Z.-X. Li, X. Zhu, Time-varying system identification using a newly improved HHT algorithm, Comput. Struct. 87 (23–24) (2009) 1611–1623.
[23] C. Fendzi, N. Mechbal, M. Rebillat, M. Guskov, G. Coffignal, A general Bayesian framework for ellipse-based and hyperbola-based damage localization in anisotropic composite plates, J. Intell. Mater. Syst. Struct. 27 (3) (2016) 350–374.
[24] G. Yan, A Bayesian approach for damage localization in plate-like structures using Lamb waves, Smart Mater. Struct. 22 (3) (2013) 035012.
[25] M.S. Salmanpour, Z. Sharif Khodaei, M. Aliabadi, Impact damage localisation with piezoelectric sensors under operational and environmental conditions, Sensors 17 (5) (2017) 1178.
[26] B. Xu, L. Yu, V. Giurgiutiu, Advanced methods for time-of-flight estimation with application to lamb wave structural health monitoring, Proc. International Workshop on SHM (2009) 1202–1209.
[27] L. Peralta, X. Cai, P. Laugier, Q. Grimal, A critical assessment of the in-vitro measurement of cortical bone stiffness with ultrasound, Ultrasonics 80 (2017) 119–126.
[28] E.B. Flynn, M.D. Todd, P.D. Wilcox, B.W. Drinkwater, A.J. Croxford, Maximum-likelihood estimation of damage location in guided-wave structural health monitoring, Proceedings of the Royal Society of London A: Mathematical, Physical and Engineering Sciences, vol. 467, The Royal Society, 2011, pp. 2575–2596.
[29] L. Yu, Z. Su, Application of kernel density estimation in Lamb wave-based damage detection, Math. Prob. Eng. (2012).

[30] E.D. Niri, S. Salamone, A probabilistic framework for acoustic emission source localization in plate-like structures, Smart Mater. Struct. 21 (3) (2012) 035009.
[31] G. Rus, J. Chiachío, M. Chiachío, Logical inference for inverse problems, Inverse Prob. Sci. Eng. 24 (3) (2016) 448–464.
[32] J.L. Beck, Bayesian system identification based on probability logic, Struct. Control Health Monit. 17 (7) (2010) 825–847.
[33] E.T. Jaynes, Information theory and statistical mechanics, Phys. Rev. 106 (4) (1957) 620.
[34] J.L. Beck, K.M. Zuev, Asymptotically independent Markov sampling: a new Markov chain Monte Carlo scheme for Bayesian inference, Int. J. Uncertainty Quantif. 3 (5) (2013).
[35] K.M. Zuev, J.L. Beck, Global optimization using the asymptotically independent Markov sampling method, Comput. Struct. 126 (2013) 107–119.
[36] H. Jeong, Y.-S. Jang, Wavelet analysis of plate wave propagation in composite laminates, Compos. Struct. 49 (4) (2000) 443–450.
[37] M. Niethammer, L.J. Jacobs, J. Qu, J. Jarzynski, Time-frequency representations of Lamb waves, J. Acoust. Soc. Am. 109 (5) (2001) 1841–1847.
[38] M.S. Arulampalam, S. Maskell, N. Gordon, T. Clapp, A tutorial on particle filters for online nonlinear/non-Gaussian Bayesian tracking, IEEE Trans. Signal Process. 50 (2) (2002) 174–188.
[39] N. Metropolis, A.W. Rosenbluth, M.N. Rosenbluth, A.H. Teller, E. Teller, Equation of state calculations by fast computing machines, J. Chem. Phys. 21 (6) (1953) 1087–1092.
[40] W.K. Hastings, Monte Carlo sampling methods using Markov chains and their applications, Biometrika 57 (1) (1970) 97–109.
[41] J.-B. Ihn, F.-K. Chang, Pitch-catch active sensing methods in structural health monitoring for aircraft structures, Struct. Health Monit. 7 (1) (2008) 5–19.
[42] F. Liang, C. Liu, J. Chuanhai, Advanced Markov Chain Monte Carlo Methods, Wiley Online Library, 2010.
[43] J. Besag, P.J. Green, Spatial statistics and Bayesian computation, J. R. Stat. Soc. Ser. B (Methodological) (1993) 25–37.
[44] T. Dursun, C. Soutis, Recent developments in advanced aircraft aluminium alloys, Mater. Des. (1980–2015) 56 (2014) 862–871.
[45] ABAQUS, Abaqus Documentation, Dassault Systemes, Providence, RI, USA, 2016.
[46] D. Alleyne, P. Cawley, A two-dimensional Fourier transform method for the measurement of propagating multimode signals, J. Acoust. Soc. Am. 89 (3) (1991) 1159–1168.
[47] M. Chiachío, J. Chiachío, G. Rus, J.L. Beck, Predicting fatigue damage in composites: a Bayesian framework, Struct. Saf. 51 (2014) 57–68.
[48] A. Gelman, G. Roberts, W. Gilks, Efficient Metropolis jumping rules, Bayesian Stat. 5 (1996) 599–608.
[49] G. Roberts, J. Rosenthal, Optimal scaling for various Metropolis-Hastings algorithms, Stat. Sci. 16 (4) (2001) 351–367.
[50] M. Gen, R. Cheng, Genetic algorithms and engineering optimization, vol. 7, John Wiley & Sons, 2000.